Autonomous Optical Navigation for Earth-Observing Satellites Using Coastline Matching

Miranda N. Straub[*] and John A. Christian[†]

West Virginia University, Morgantown, WV, 26506

In order to meet the demands of future space missions, it is beneficial for spacecraft to have the capability to support autonomous navigation. This is true for both crewed and uncrewed vehicles. For crewed vehicles, autonomous navigation would allow the crew to safely navigate home in the event of a communication system failure. For uncrewed missions, autonomous navigation reduces the demand on ground-based infrastructure and could allow for more flexible operation. One promising technique for achieving these goals is through optical navigation. To this end, the present work considers how camera images of the Earth's surface could enable autonomous navigation of a satellite in low Earth orbit. Specifically, this study will investigate the use of coastlines and other natural land-water boundaries for navigation. Observed coastlines can be matched to a pre-existing coastline database in order to determine the location of the spacecraft. This paper examines how such measurements may be processed in an on-board Extended Kalman Filter (EKF) to provide completely autonomous estimates of the spacecraft state throughout the duration of the mission.

Nomenclature

J Jacobian Matrix
f Residual value vector
x Variable value vector
F Force, N
m Mass, kg
Δx Variable displacement vector
α Acceleration, m/s^2

Subscript
i Variable number

I.   Introduction

With the many recent technological developments in the aerospace industry and the desire to conduct more ambitious space missions, there is an increasing need for fully autonomous spacecraft. Autonomous spacecraft navigation systems are important for crewed and uncrewed missions. In the case of crewed missions, autonomous navigation systems are crucial in bringing the crew home safely in case of a communication system failure. For either scenario, previous work has shown optical navigation to be one method of fulfilling the need for autonomous navigation.[1]

The process of optical navigation includes capturing an image of a known object and using the information in this image to determine the location of the spacecraft. Target bodies for optical navigation include planets, planetary satellites, asteroids, comets and stars.[2] At closer ranges, surface features may be observed. On

---

[*]Graduate Research Assistant, Department of Mechanical and Aerospace Engineering, Benjamin M. Statler College of Engineering and Mineral Resources.

[†]Assistant Professor, Department of Mechanical and Aerospace Engineering, Benjamin M. Statler College of Engineering and Mineral Resources, and AIAA Senior Member.

Earth these surface features include coastlines, islands, and other in-land water boundaries such as lakes and rivers.[3] Thus, the focus of this paper will be on autonomous optical navigation of a satellite in low-Earth orbit (LEO) using coastlines as landmarks.

For this study, it is assumed that the only source of external measurements will be from a star-tracker (for attitude) and from an Earth-observing camera. The state of the spacecraft will be propagated on-board using assumed dynamics and Inertial Measurement Unit (IMU) data. In addition, a camera measurement model will be developed to utilize measurements obtained from landmark observations to be processed in an on-board Extended Kalman Filter (EKF). These models will be discussed in detail later in the paper.

I.A. Navigation Using Landmarks

Many studies have been carried out concerning the use of optical navigation with various surface landmarks as targets. For example, craters commonly found on the surface of planets, satellites, asteroids, and other solar system bodies are often proposed as landmarks for optical navigation.[4-8] Generally, a crater can be identified in an image by looking for an elliptical rim and a bright to dark shading pattern depending on the lighting at the time of observation. Because of these commonalities, most crater detection algorithms consist of a series of steps that include edge detection and ellipse fitting. Once the ellipses are identified as landmarks, the size, shape, and position of that landmark relative to other landmarks are used to match the ellipses with a known database of craters for that body.[6] It should be noted, however, that this process can be difficult because the craters often have different appearances when viewed from different directions and with different sun angles. Also, the age of the crater may contribute to the sharpness of the crater edges on the surface which can make detection easier or more difficult.[4] Techniques such as image cross-correlation, context based matching, and projective conic invariants can be used to make up for these differences but are beyond the scope of this paper. They are discussed in detail in [4] and [8].

Due to the previously mentioned irregularities seen in crater detection, and because craters are less numerous on the Earth's surface, bodies of water can also be used as landmarks for spacecraft orbiting Earth in LEO. This is easily observed due to the contrast in colors between land and water as seen by the spacecraft. These bodies of water can include coastlines, islands, rivers, and lakes. Additional features can be detected as well (e.g. volcanoes, mountains, snow, and even urban areas); however these are often changing over time and can be more difficult to distinguish and map.[9]

I.B. Coastline Determination

Numerous methods of extracting coastlines from images have been studied. Common solutions include using conventional image processing boundary detection methods or classifying illumination levels of an image. When using boundary or edge detection, various methods are available and produce similar results depending on the situation. One popular choice for edge detection is the Canny edge detector.[10] Previous work by Liu and Jezek,[3] however, has shown Canny edge detection to be insufficient for coastline extraction due to the lack of consistent intensity contrast between land and water regions often resulting in discontinuous coastline data. To alleviate this problem, image segmentation and post-segmentation processing were used in [3]. Other authors, such as those in [11], use two additional masking steps in addition to the Canny edge detection: an additional edge focusing step and a closing step used as an input for the object-oriented matching process. These additional steps greatly helped automate the extraction of coastlines from the images used.

An additional problem that arises with coastline extraction and feature selection is the accuracy of determining actual coastlines. For example, many edge detection techniques use contrast as a determining factor to differentiate boundaries and edges. If the satellite image contains cloud coverage, it is possible for clouds to be considered boundaries and therefore identified as coastlines. A solution to this problem was discussed in [12] using a global ocean color sensor which measures radiances in eight visible and near-infrared bands. By creating scatter plots of radiance observed from two different bands, it was possible to normalize the data and specify thresholds to classify observed regions as land, water, clouds, or ice.

I.C. Georeferenced Database

A few options are available to provide a reference of coastlines for optical navigation. One of the most well-known databases is provided by the National Geophysical Data Center (NGDC), part of the National Oceanic

and Atmospheric Administration (NOAA). World shorelines are provided through the Global Self-Consistent, Hierarchical, High-resolution Geography Database (GSHHG) in the form of shapefiles. A shapefile stores geometric location and attribute information for spatial features in a data set where the geometry of a feature is stored as a shape comprising of a set of vector coordinates.[13] Shapefiles can support point, line, and area features which allow for coastline and other water/land boundaries to be stored. These files are able to be read and written using a variety of programs. The NGDC provides a software called GEODAS-NG that has the capability of reading the coastline data from the GSHHG or writing shapefiles from a provided input image.

It is also possible to use MATLAB as a georeferenced database in conjunction with the GSHHG database. MATLAB is capable of plotting the data with respect to latitude and longitude coordinates. To simulate this concept, MATLAB was used to construct a model of the Earth as viewed by a satellite in a 1,000 km near-polar orbit. A near-polar orbit was chosen in order to ensure most of the Earth's surface is observed. The footprint simulation was modeled under the assumption that the on-board camera is always nadir-pointing. With this assumption, the spacecraft position vectors were calculated using basic orbital mechanics equations and used as the position of the camera. Figure 2 shows an example of this simulation.
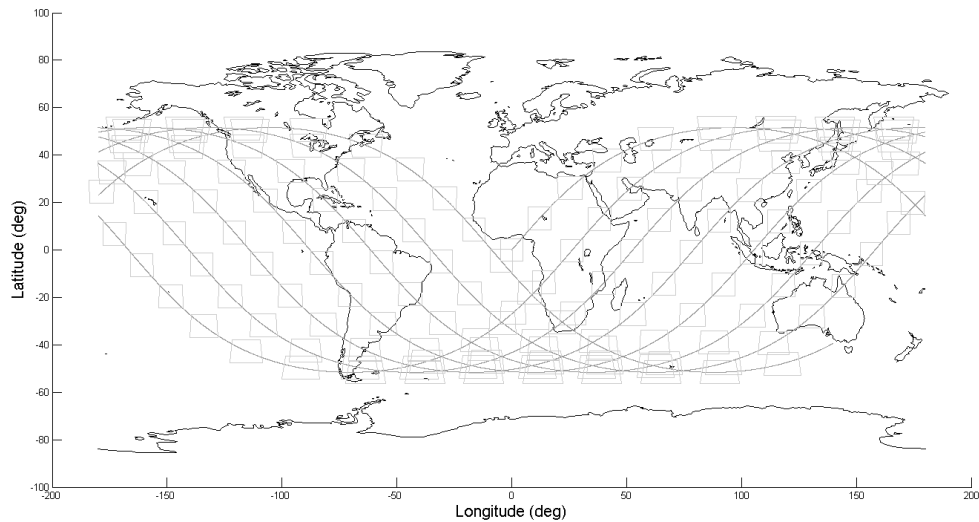

Figure 1: Coastlines visible at 56°inclination and 1000 km altitude when images are taken once every 5 minutes

A ground projected field-of-view (GFOV) was calculated based on the geometry of the satellite position and desired field-of-view (FOV) of the camera,

$$GFOV = 2h \tan\left(\frac{FOV}{2}\right) \tag{1}$$

where h is the spacecraft altitude. A 30° FOV was chosen resulting in a viewable footprint of approximately 536 km as seen in Fig. 2a.

II.   Mathematical Models

In order to create an algorithm for optical navigation, it is necessary to understand the mathematical models describing the state of the spacecraft as well as the camera model. These models are described in the following sections.

II.A.   Extended Kalman Filter

Due to the nonlinear nature of spacecraft dynamics and optical measurements, an Extended Kalman Filter (EKF) will be used to estimate the state of the system.[14, 15] The key equations are now briefly reviewed.

American Institute of Aeronautics and Astronautics
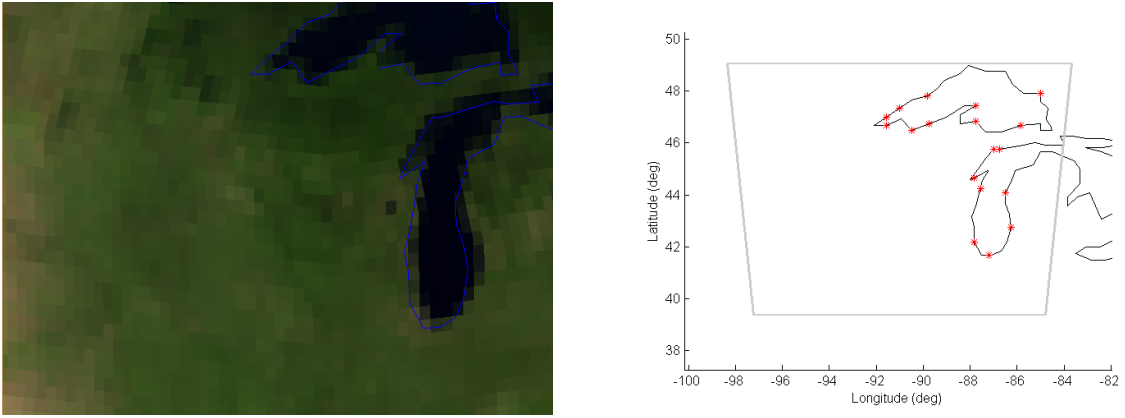
(a) Satellite image with overlay of coastlines from MAT-LAB database

(b) MATLAB coastline model with identified coastline points (o) and spacecraft position (*)

Figure 2: MATLAB simulated satellite view and identified coastline points within spacecraft FOV

Suppose we have a nonlinear system governed by

$$\dot{\mathbf{x}} = \mathbf{f}(\mathbf{x}, t) + \mathbf{v} \tag{2}$$

where $\mathbf{v}$ is zero mean white noise. The covariance of such a system may be propagated by

$$\dot{\mathbf{P}} = \mathbf{F}\mathbf{P} + \mathbf{P}\mathbf{F}^T + \mathbf{Q} \tag{3}$$

where

$$\mathbf{F}(t) = \left.\frac{\partial \mathbf{f}(\mathbf{x}, t)}{\partial \mathbf{x}}\right|_{\mathbf{x}=\hat{\mathbf{x}}} \tag{4}$$

Further suppose that at some time, t_k, a new measurement becomes available that is described by

$$\tilde{\mathbf{y}}_k = \mathbf{h}(\mathbf{x}_k) + \mathbf{u}_k \tag{5}$$

where $\mathbf{u}_k \sim \mathcal{N}(0, \mathbf{R}_k)$ and $\mathbf{h}(\mathbf{x})$ is the nonlinear measurement model.

Both the *a posteriori* state and covariance estimates, $\hat{\mathbf{x}}_k^+$ and $\mathbf{P}_k^+$, may now be computed by

$$\hat{\mathbf{x}}_k^+ = \hat{\mathbf{x}}_k^- + \mathbf{K}_k(\tilde{\mathbf{y}}_k - \mathbf{h}(\hat{\mathbf{x}}_k^-)) \tag{6}$$

$$\mathbf{P}_k^+ = (\mathbf{I} - \mathbf{K}_k\mathbf{H}_k)\mathbf{P}_k^-(\mathbf{I} - \mathbf{K}_k\mathbf{H}_k)^T + \mathbf{K}_k\mathbf{R}_k\mathbf{K}_k^T \tag{7}$$

where $\mathbf{H}_k$ is the measurement sensitivity matrix,

$$\mathbf{H}_k \triangleq \left.\frac{\partial \mathbf{h}(\mathbf{x})}{\partial \mathbf{x}}\right|_{\mathbf{x}=\hat{\mathbf{x}}} \tag{8}$$

Finally, the optimal update is achieved when $\mathbf{K}_k$ is chosen to be the Kalman gain,

$$\mathbf{K}_k = \mathbf{P}^-\mathbf{H}_k^T(\mathbf{H}_k\mathbf{P}\mathbf{H}_k^T + \mathbf{R}_k)^{-1} \tag{9}$$

II.B. State Propagation using an Extended Kalman Filter

To estimate the state of the spacecraft, the dynamics can be expressed using two-body problem orbital mechanics. The resulting equations of motion for the spacecraft are described by

$$\ddot{\mathbf{r}} = \frac{-\mu}{\|\mathbf{r}\|^3}\mathbf{r} \tag{10}$$

Rewriting in state-space form leads to the following expression for $\mathbf{f}(\mathbf{x}, t)$

$$\mathbf{x} = \begin{bmatrix} \mathbf{r} \\ \dot{\mathbf{r}} \end{bmatrix} \tag{11}$$

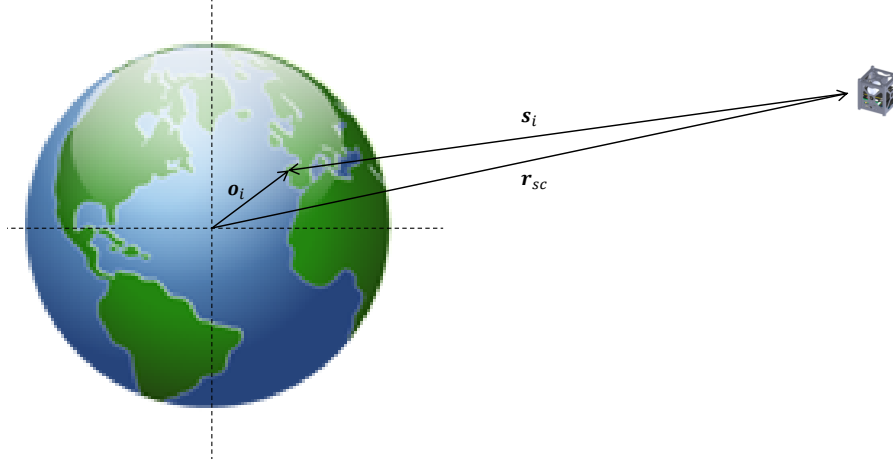American Institute of Aeronautics and Astronautics

Figure 3: Line-of-sight vectors for measurement model

$$\mathbf{f}(\mathbf{x}, t) = \begin{bmatrix} \dot{\mathbf{r}} \\ \frac{-\mu}{\|\mathbf{r}\|^3}\mathbf{r} \end{bmatrix} \tag{12}$$

Because $\ddot{\mathbf{r}}$ is nonlinear in $\mathbf{r}$, $\dot{\mathbf{x}}$ must be linearized to first order about the estimate to find $\mathbf{F}(t)$,

$$\mathbf{F}(t) = \left. \frac{\partial \mathbf{f}(\mathbf{x}, t)}{\partial \mathbf{x}} \right|_{\mathbf{x}=\hat{\mathbf{x}}} = \begin{bmatrix} \frac{\partial \dot{\mathbf{r}}}{\partial \mathbf{r}} & \frac{\partial \dot{\mathbf{r}}}{\partial \dot{\mathbf{r}}} \\ \frac{\partial \ddot{\mathbf{r}}}{\partial \mathbf{r}} & \frac{\partial \ddot{\mathbf{r}}}{\partial \dot{\mathbf{r}}} \end{bmatrix} = \begin{bmatrix} 0_{3\times3} & \mathbf{I}_{3\times3} \\ \frac{-\mu}{\|\hat{\mathbf{r}}\|^3}\mathbf{I}_{3\times3} + \frac{-\mu}{\|\hat{\mathbf{r}}\|^5}\hat{\mathbf{r}}\hat{\mathbf{r}}^T & 0_{3\times3} \end{bmatrix} \tag{13}$$

Since both $\dot{\mathbf{x}}$ and $\dot{\mathbf{P}}$ are now known, each can be integrated to propagate to a new *a priori* estimate of the state and covariance, $\hat{\mathbf{x}}_k^-$ and $\hat{\mathbf{P}}_k^-$, which are then updated by the EKF.

II.C. Measurement Model for Coastline Points in Images

Images produce line-of-sight (LOS) measurements. These measurements are a nonlinear function of the spacecraft state and may be determined by the geometry between the Earth and the spacecraft as shown in Fig. 3. From this figure, it is clear that

$$\mathbf{s}_i = \mathbf{o}_i - \mathbf{r}_{sc} \tag{14}$$

$$\mathbf{e}_{iI} = \frac{\mathbf{s}_i}{\|\mathbf{s}_i\|} \tag{15}$$

where $\mathbf{r}_{sc}$ is the position of the spacecraft from the center of the earth, $\mathbf{s}_i$ is the vector from the spacecraft to the ith point, or landmark, and $\mathbf{o}_i$ is the vector from the center of the earth to the landmark. This leads to a measurement model for a single observed coastline point

$$\mathbf{h}(\mathbf{x}) = \mathbf{e}_{iC} = \mathbf{T}_C^I \mathbf{e}_{iI} = \mathbf{T}_C^I \frac{(\mathbf{o}_i - \mathbf{r}_{sc})}{[(\mathbf{o}_i - \mathbf{r}_{sc})^T(\mathbf{o}_i - \mathbf{r}_{sc})]^{1/2}} \tag{16}$$

where $\mathbf{T}_C^I$ is the rotation matrix from the inertial frame to the camera frame. From here, the measurement sensitivity matrix may be computed as

$$\mathbf{H}_i = \mathbf{T}_C^I \frac{1}{\|\mathbf{o}_i - \mathbf{r}_{sc}\|} \left[\{\mathbf{e}_{iI}\mathbf{e}_{iI}^T - \mathbf{I}_{3\times3}\} \quad \mathbf{0}_{3\times3} \right] \tag{17}$$

In order to update the state measurement, the measurement covariance, $\mathbf{R}_i$, needs to be determined to calculate the Kalman Gain, as seen in Eq. 9. This can be determined to first order using the QUEST covariance matrix, as is common practice with unit vector measurements,[16]

$$\mathbf{R}_i = E[(\mathbf{e}_{iC} - \bar{\mathbf{e}}_{iC})(\mathbf{e}_{iC} - \bar{\mathbf{e}}_{iC})^T] \approx \sigma_\Theta^2(\mathbf{I}_{3\times3} - \bar{\mathbf{e}}_{iC}\bar{\mathbf{e}}_{iC}^T) \tag{18}$$

American Institute of Aeronautics and Astronautics

It should be noted that in order to calculate the Kalman gain, $\mathbf{H}_i \mathbf{PH}_i^T + \mathbf{R}_i$ must be invertible. In this particular case, the null space of $\mathbf{R}_i$ is the same as the null space of $\mathbf{H}_i \mathbf{PH}_i^T$. This causes the matrix to be non-invertible (a 3×3 matrix with rank 2). To avoid numerical issues in calculations, the Kalman gain equation can be adjusted by adding a rank-one matrix where $\nu \mathbf{e}_i \mathbf{e}_i^T$.[17]

$$\mathbf{K}_i = \mathbf{P}^- \mathbf{H}_i^T (\mathbf{H}_i \mathbf{PH}_i^T + \mathbf{R}_i + \nu \mathbf{e}_i \mathbf{e}_i^T)^{-1} \tag{19}$$

In Eq. 9, $\nu = 0.5 tr[\mathbf{R}_i]$ is chosen to ensure the matrix we are inverting is well conditioned. As explained in [17], this does not change the value of $\mathbf{K}_i$ since it is equivalent to adding a $\mathbf{0}$ to the overall equation,

$$\mathbf{H}_i^T \mathbf{e}_i = 0 \tag{20}$$

III.   Results

For this simulation, it is important to ensure that coastlines will be visible based on the spacecraft's orbit and camera parameters. Therefore, simulations were run to determine the percentage of time coastlines would be visible from the spacecraft's position in a 1000km circular orbit with varying inclinations. For simplicity, other orbital parameters, including the right ascension of the ascending node, the argument of periapsis, and the true anomaly, were fixed at 0 radians. As a result, Fig. 4 was produced to show the results based on varying inclinations as well as varying camera FOVs. It is important to note that these results are orbit-specific and will vary slightly due to differences in orbital parameters specific to a satellite's orbit. Consequently, the rate at which images are captured also plays a key role in determining how often coastlines are observable. In this case, images are to be taken once every five minutes for a total of twelve hours.
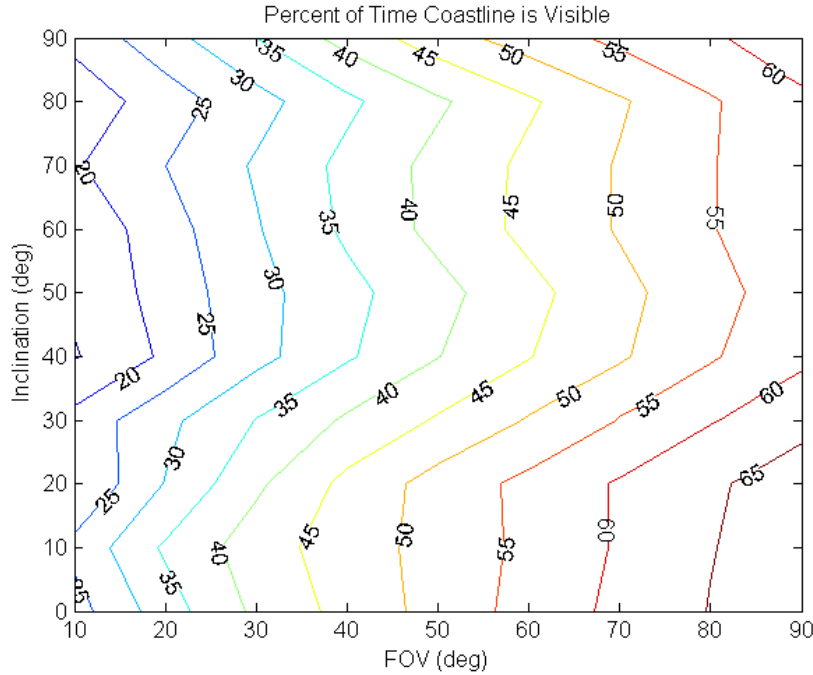

Figure 4: Orbit-specific contour plot showing the percentage of time coastline is observable based on inclination and FOV at a 1000km circular orbit with images taken once every five minutes.

III.A.   Assessment of Navigation Filter Performance

This section discusses the results obtained from simulated data at a 1000 km altitude circular orbit. Results from the Extended Kalman Filter were analyzed for three different inclinations of 0°(equatorial orbit), 45°, and 90°(polar orbit). All simulations were done with a FOV of 30°.
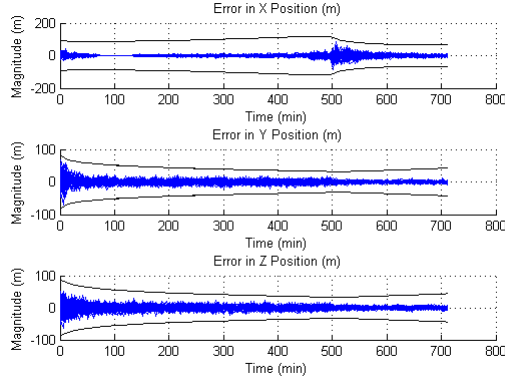
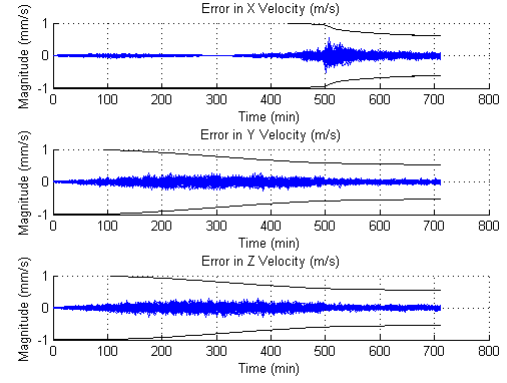American Institute of Aeronautics and Astronautics
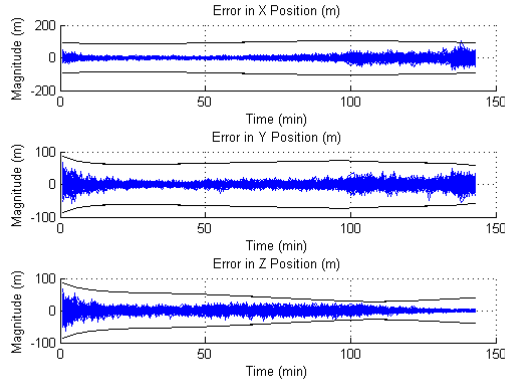
(a) Position Error at i=90°
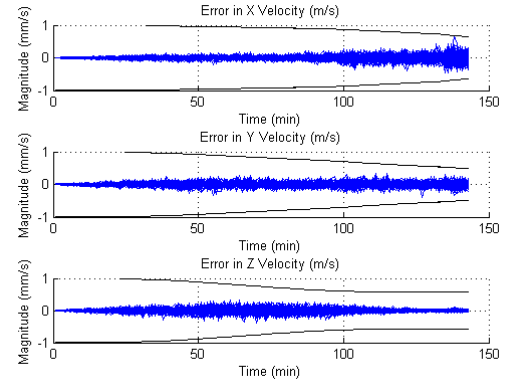
(b) Velocity Error at i=90°

Figure 5: Monte Carlo Position and Velocity Errors at 1000km polar orbit

(a) Position Error at i=90°
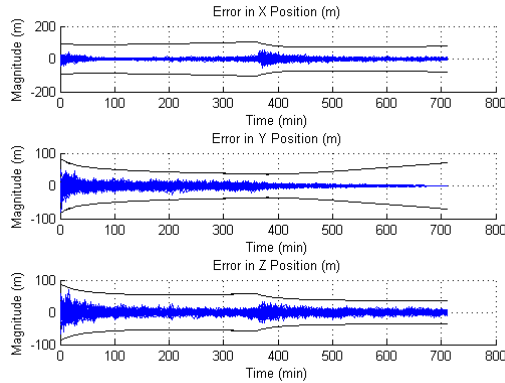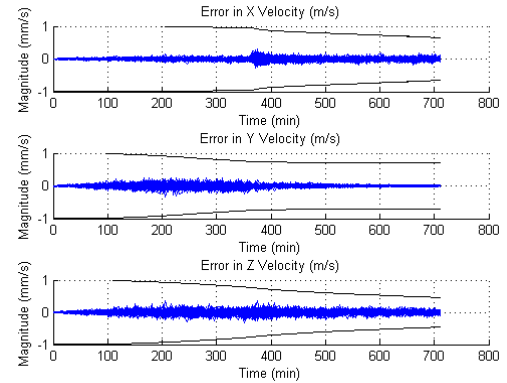
(b) Velocity Error at i=90°

Figure 6: Monte Carlo Position and Velocity Errors at 1000km 45 °orbit

(a) Position Error at i=90°

(b) Velocity Error at i=90°

Figure 7: Monte Carlo Position and Velocity Errors at 1000km 0 °orbit

IV.   Acknowledgments

References

[1] Christian, J. A. and Lightsey, E. G., "Onboard Image-Processing Algorithm for a Spacecraft Optical Navigation Sensor System," *Journal of Spacecraft and Rockets*, Vol. 49, No. 2, 2012, pp. 337–352.

[2] Owen, W., "Methods of Optical Navigation," *AAS Spaceflight Mechanics Conference*, No. AAS 11-215, New Orleans, LA, February 2011.

[3] Liu, H. and Jezek, K. C., "Automated Extraction of Coastline from Satellite Imagery by Integrating Canny Edge Detection and Locally Adaptive Thresholding Methods," *International Journal of Remote Sensing*, Vol. 25, No. 5, 2004, pp. 937–958.

[4] Cheng, Y. and Miller, J. K., "Autonomous Landmark Based Spacecraft Navigation System," *AAS/AIAA Astrodynamics Specialist Conference*, No. AAS 03-223, Ponce, Puerto Rico, February 2003.

[5] Rowell, N., Parkes, S., and Dunstan, M., "Image Processing for Near Earth Object Optical Guidance Systems," *IEEE Transactions on Aerospace and Electronic Systems*, Vol. 49, No. 2, 2013, pp. 1057–1072.

[6] Hanak, C., *Lost in Low Lunar Orbit Crater Pattern Detection and Identification*, Ph.D. thesis, University of Texas at Austin, 2009.

[7] Rohrschneider, R. R., "Terrain Relative Navigation Using Crater Identification in Surface Topography Data," *AIAA Guidance, Navigation, and Control Conference*, No. AIAA 2001-6490, Portland, Oregon, August 2011.

[8] Cheng, Y., Johnson, A. E., Matthies, L. H., and Olson, C. F., "Optical Landmark Detection for Spacecraft Navigation," *AAS/AIAA Astrodynamics Specialist Conference*, No. AAS 02-224, Ponce, Puerto Rico, February 2003.

[9] National Aeronautics and Space Administration, "Earth Features Seen From Space," May 1999.

[10] Canny, J., "A Computational Approach to Edge Detection," *IEEE Transactions on Pattern Analysis and Machine Intelligence*, Vol. 8, No. 6, 1986, pp. 679–698.

[11] Heene, G. and Gautama, S., "Optimisation of a Coastline Extraction Algorithm for Object-Oriented Matching of Multi-sensor Satellite Imagery," *IEEE Geoscience and Remote Sensing Symposium*, Vol. 6, 2000, pp. 2632–2634.

[12] Patt, F. S., Woodward, R. H., and Gregg, W. W., "An Automated Method for Navigation Assessment for Earth Survey Sensors using Target Islands," *International Journal of Remote Sensing*, Vol. 18, No. 16, 1997, pp. 3311–3336.

[13] Environmental Systems Research Institute, I., "ESRI Shapefile Technical Description," 1998.

[14] Gelb, A., *Applied Optimal Estimation*, The M.I.T. Press, Cambridge, MA, 1974.

[15] Brown, R. G. and Hwang, P. Y. C., *Introduction to Random Signals and Applied Kalman Filtering*, John Wiley and Sons, Inc., Hoboken, NJ, 1997.

[16] Shuster, M. D. and Oh, S. D., "Three-axis Attitude Determination from Vector Observations," *Journal of Guidance, Control, and Dynamics*, Vol. 4, No. 1, 1981, pp. 70–77.

[17] Liounis, A., Daniel, S., and Christian, J. A., "Autonomous Navigation System Performance in the Earth-Moon System," *AIAA Space Conference*, 2013.

American Institute of Aeronautics and Astronautics